

Emergent orbitals in the cluster Mott insulator on a breathing Kagome lattice

Gang Chen^{1,2} and Patrick A. Lee³

¹State Key Laboratory of Surface Physics, Department of Physics,

Center for Field Theory & Particle Physics, Fudan University, Shanghai, 200433, China

²Collaborative Innovation Center of Advanced Microstructures, Nanjing, 210093, China and

³Department of Physics, Massachusetts Institute of Technology, Cambridge, Massachusetts, 02139, United States

(Dated: May 16, 2018)

Motivated by the recent developments on cluster Mott insulating materials such as the cluster magnet $\text{LiZn}_2\text{Mo}_3\text{O}_8$, we consider the strong plaquette charge ordered regime of the extended Hubbard model on a breathing Kagome lattice and reveal the properties of the cluster Mottness. The plaquette charge order arises from the inter-site charge interaction and the collective motion of three localized electrons on the hexagon plaquettes. This model leads naturally to a reduction of the local moments by $2/3$ as observed in $\text{LiZn}_2\text{Mo}_3\text{O}_8$. Furthermore, at low temperatures each hexagon plaquette contains an extra orbital-like degree of freedom in addition to the remaining spin $1/2$. We explore the consequence of this emergent orbital degree of freedom. We point out the interaction between the local moments is naturally described by a Kugel-Khomskii spin-orbital model. We develop a parton approach and suggest a spin liquid ground state with spinon Fermi surfaces for this model. We further predict an emergent orbital order when the system is under a strong magnetic field. Various experimental consequences for $\text{LiZn}_2\text{Mo}_3\text{O}_8$ are discussed, including an argument that the charge ordering much be short ranged if the charge per Mo is slightly off stoichiometry.

I. INTRODUCTION

Spin, charge, and orbital are three basic degrees of freedom of condensed matter systems, and their mutual interaction, interplay, and entanglement cover the major topics of modern condensed matter physics¹⁻⁴. In conventional Mott insulators, the electron charge localization creates the local spin moments at the lattice sites, and the orbital degree of freedom becomes active when the local crystal symmetry allows the degeneracy of the atomic orbitals³. Recently, the cluster Mott insulator emerge as a new type of Mott insulator in which the electrons are localized inside the cluster⁵⁻¹³. As a result, the keen interplay between the charge and the spin degrees of freedom in cluster Mott insulators (CMI) is often quite different from the conventional Mott insulator⁵⁻⁸. In particular, it was shown that the two-dimensional CMI of the Kagome system^{6,8} with an extended Hubbard model at the $1/6$ electron filling may develop a plaquette charge order¹⁴⁻¹⁸ on the hexagon plaquette (see Fig. 1). This plaquette charge order immediately impacts the spin degree of freedom and modulates the spin properties by reconstructing the spin state within each plaquette. Such a charge-driven spin-state-reconstruction is one crucial property of the CMI in this system⁶.

Well known examples of the cluster magnets include $\text{LiZn}_2\text{Mo}_3\text{O}_8$, $\text{Li}_2\text{InMo}_3\text{O}_8$ ¹⁹, and $\text{ScZnMo}_3\text{O}_8$ ²⁰, where the Mo electrons are in the CMI with the Mo electrons localized in the smaller triangular clusters of the distorted Kagome lattice (see Fig. 1)²¹⁻²⁵. The distortion is such that the up and down triangles have different bond lengths and the lattice is often referred to as the breathing kagome. Interestingly, the material $\text{LiZn}_2\text{Mo}_3\text{O}_8$ experiences two Curie regimes with distinct Curie-Weiss temperatures and Curie constants^{22,23} in which the low temperature Curie constant is $1/3$ of the high tempera-

ture one and the low temperature Curie-Weiss temperature is much smaller than the high temperature one. Moreover, the system remains magnetically disordered down to the lowest measured temperature, and the inelastic neutron scattering does observe a continuum of excitations²¹. This is consistent with the proposal of spin liquid ground state in this material. Partly inspired by the experiments in $\text{LiZn}_2\text{Mo}_3\text{O}_8$, we here explore the strong plaquette charge ordered regime of the CMI on the breathing Kagome system where the electron charges are localized on the resonating hexagon plaquettes (see Fig. 1). In addition to the on-site repulsion, a large inter-site repulsion is assumed which forbids the occupation of neighboring sites. This leads to plaquette charge ordering

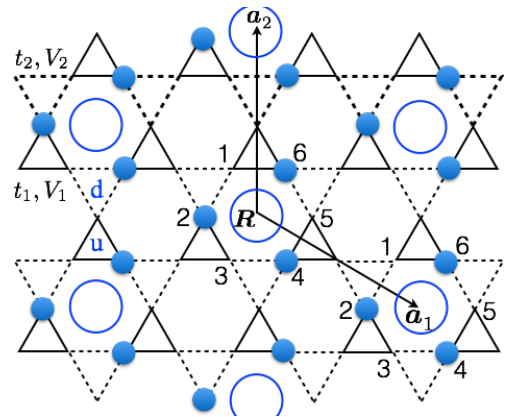


FIG. 1. (Color online.) The breathing Kagome lattice with plaquette charge order. The solid (dashed) lines represent the up (down) triangles. The plaquette charge order hosts three electrons that are resonating on the hexagons with circles marked, and $\mathbf{a}_1, \mathbf{a}_2$ are two lattice vectors that connect neighboring resonating hexagons. ' \mathbf{R} ' labels the resonating hexagon, and '1,2,3,4,5,6' label the six vertices.

and the expansion of the unit cell, formed by a triangular lattice of hexagons marked by the circles in Fig 1. The low lying degree of freedom is the collective resonant rotation of the three occupied sites on each hexagon (see Fig. 2). To put this model in context of the earlier model by Flint and Lee²⁶, there the inter-site repulsion is assumed to be weak and each up triangle is occupied by one electron, and no correlation is assumed around the hexagons. The up triangles form a triangular lattice and a lattice distortion is postulated which creates a honeycomb lattice of up triangles, with the spin at the center of the honeycomb relatively isolated and responsible for the local moments at low temperatures. Note that both for this model and the current model, a tripling of the unit cell is assumed. This has been searched for by X-ray scattering but so far no new diffraction peaks have been observed. This issue will be discussed in the Discussion section, where we point out that if the system is slightly off stoichiometry, domain walls will form between the ordered states. Due to a special feature of domain walls forming a honeycomb lattice²⁷, it can be shown that long range order is always destroyed, *i.e.* the system can only have short range order. This may help explain the absence of new diffraction spots and both models may remain viable. We also point out that in the Flint-Lee model addressed only the freeze out of 2/3 of the spins at low temperatures, and the ultimate fate of the local moments that remained was not discussed. In the current model, we address both the freeze out and the true ground state of this system and argue that due to an emergent orbital degree of freedom, a spin liquid state may form as the true ground state.

We also compare the current paper with a previous work on a similar model⁶ which treats the weak plaquette order regime. The current treatment of the CMI is analogous to the strong Mott regime of a conventional Mott insulator, while the previous weak plaquette charge ordered regime⁶ is like the weak Mott regime (ie close to the Mott transition) where the charge fluctuation may destabilize the spin order and lead to a spin liquid^{28,29}. We find that in the strong charge ordered regime, the charge-spin interaction appears in a much more straightforward and transparent manner. We explain the local moment reconstruction in the presence of the strong plaquette charge order on the hexagon, giving rise to a net spin-1/2 local moment on the hexagon. We point out that there exists an emergent orbital-like degree of freedom. This emergent orbitals are two-fold degenerate and protected by the symmetry of the hexagon plaquette. The natural model, that describes the interaction between the effective spin and the emergent orbital on the hexagon plaquette, is the Kugel-Khomskii exchange model³⁰. As a comparison with the conventional Mott insulators, the Kugel-Khomskii model is used to describe the exchange interaction between the local moments when there exists an orbital degeneracy for the atomic orbitals³⁰.

For the Kugel-Khomskii model, we design a fermionic parton approach to represent the effective spin and the

emergent orbital degrees of freedom, and propose a spinon Fermi surface spin liquid ground state. We point out that the emergent orbital generically creates non-degenerate spinon bands and allows inter-band particle-hole excitations. Specifically, the inter-band particle-hole excitations would manifest as a finite-energy spinon continuum at the Γ point in the inelastic neutron scattering and the optical measurement. Polarizing the spin degrees of freedom by applying strong magnetic fields, we obtain a simple 120-degree compass model for the emergent orbital interaction. We further predict that the system selects a specific orbital order via order by quantum disorder and supports a nearly gapless pseudo-Goldstone mode. These results establish a new perspective on the Mottness of the CMI.

The following part of the paper is organized as follows. In Sec. II, we introduce the extended Hubbard model and explain the plaquette charge order. In Sec. III, we explain the local moment structure of the resonating hexagon in the strong plaquette charge ordered regime and point out the fundamental existence of the emergent orbital degree of freedom. In Sec. IV, we derive the Kugel-Khomskii model that describes the exchange interaction between the spin and the orbital on the triangular lattice formed by the resonating hexagons. In Sec. V, we design a parton construction and suggest the features of the spinon continuum for the proposed spinon Fermi surface ground state. In Sec. VI, we explain the emergent orbital order, quantum order by disorder effect of the compass model for the orbitals, and the orbital excitation when the spin is polarized by the external magnetic field. In Sec. VII, we discuss the relevance of this model to $\text{LiZn}_2\text{Mo}_3\text{O}_8$ and explore various experimental consequences. We end with a broad view on the cluster Mott insulating materials.

II. THE MICROSCOPIC MODEL AND THE PLAQUETTE CHARGE ORDER

We start with the extended Hubbard model on the breathing Kagome lattice (see Fig. 1),

$$H = - \sum_{\langle ij \rangle \in \text{u}} (t_1 c_{i\sigma}^\dagger c_{j\sigma} + h.c.) - \sum_{\langle ij \rangle \in \text{d}} (t_2 c_{i\sigma}^\dagger c_{j\sigma} + h.c.) + \sum_{\langle ij \rangle \in \text{u}} V_1 n_i n_j + \sum_{\langle ij \rangle \in \text{d}} V_2 n_i n_j + \sum_i U n_{i\uparrow} n_{i\downarrow}, \quad (1)$$

where $c_{i\sigma}^\dagger$ ($c_{i\sigma}$) creates (annihilates) an electron with spin σ ($=\uparrow, \downarrow$) at the lattice site i , n_i ($\equiv n_{i\uparrow} + n_{i\downarrow}$) is the electron occupation number, and ‘u’ and ‘d’ refer to the up and down triangles that are of different sizes, respectively. Here, t_1 and V_1 (t_2 and V_2) are the electron hopping and repulsion on neighboring sites of the up (down) triangles, respectively. The electron filling is 1/6, *i.e.* one electron per unit cell on the breathing Kagome lattice. This model was suggested to capture the physics of the Mo-based

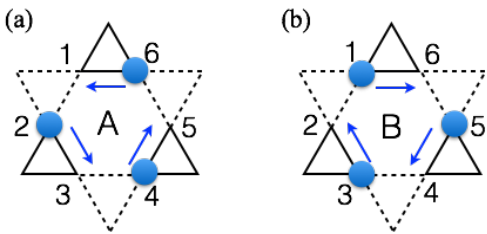


FIG. 2. (Color online.) The correlated and collective motion of the three electrons on the elementary hexagon. Arrow indicates the hopping direction. Note that the hoppings of the three electrons happen at the same time.

cluster magnets such as $\text{LiZn}_2\text{Mo}_3\text{O}_8$ in which the Mo atoms form an breathing Kagome lattice^{6,19,20}.

The Hubbard U interaction for our system merely removes the electron double occupancy on the lattice site, but cannot localize the electrons on the lattice sites. The electrons can move on the lattice without encountering any double occupancy. This is quite different from the conventional Mott insulator where the electrons are localized on the lattice sites. It is the inter-site interactions, V_1 and V_2 , that localize the electron on the triangular clusters of the Kagome system. Despite being localized on the triangular clusters, the electrons manage to fluctuate in a collective fashion due to the extensive degeneracy of the electron occupation configuration on the Kagome lattice. As U is often quite large compared to t_1, t_2, V_1, V_2 , one could safely ignore the electron configurations with any double occupancy. With a third-order degenerate perturbation of the electron hoppings, we obtain an effective Hamiltonian that operates on the degenerate electron occupation manifold and is given as⁶

$$H_{\text{eff}} = - \sum_{\square} \sum_{\alpha\beta\gamma} [K_1 (c_{1\alpha}^\dagger c_{6\alpha} c_{5\beta}^\dagger c_{4\beta} c_{3\gamma}^\dagger c_{2\gamma} + h.c.) + K_2 (c_{1\alpha}^\dagger c_{2\alpha} c_{3\beta}^\dagger c_{4\beta} c_{5\gamma}^\dagger c_{6\gamma} + h.c.)], \quad (2)$$

where we have

$$K_1 = 6t_1^3/V_2^2, \quad K_2 = 6t_2^3/V_1^2, \quad (3)$$

and “1,2,3,4,5,6” refer to the six vertices on the elementary hexagon of the Kagome lattice. H_{eff} describes the correlated and collective motion of the three electrons on the elementary hexagon (see Fig. 2). By mapping the electron occupation to the dimer covering on the dual honeycomb lattice^{6,31}, the previous work has obtained a plaquette charge order where the electrons preferentially occupy 1/3 of the hexagons in a periodic fashion (see Fig. 1)^{6,16–18,32}. This plaquette charge order is a quantum effect because the three electrons are resonating on the hexagons and form a linear superposition of the two occupation configurations⁶. In the strong plaquette charge ordered limit, the electron (charge) occupation wavefunction would be well approximated by a

simple product state with

$$|\Psi\rangle_c = \prod_{\mathbf{R}} \frac{1}{\sqrt{2}} [|\circ_{\mathbf{R}}\rangle_A + |\circ_{\mathbf{R}}\rangle_B], \quad (4)$$

where \mathbf{R} refers to the position of the resonating hexagons, and A and B label the two charge occupation configurations of the three electrons on the resonating hexagon (see Fig. 1). The spin quantum number can still be transferred via the spin exchange interaction, so $|\Psi\rangle_c$ merely represents the charge wavefunction.

III. THE EMERGENT ORBITALS AND THE LOCAL MOMENTS

In this section, we focus on the strong plaquette charge ordered regime and reveal the novel features of the local moment structure. The three electrons are well localized on the resonating hexagons but still move in the collective fashion that is governed by H_{eff} . This collective motion tunnels the electron spins that are interacting with the superexchange interaction at the same time. As a comparison, the localized electrons on a lattice site of a conventional Mott insulator are fully governed by the atomic electron interactions and the Hund’s rules. Here, the right model that describes the localized electrons on an individual resonating hexagon is

$$H_{\circ_{\mathbf{R}}} = -K_1 \sum_{\alpha\beta\gamma} (c_{1\alpha}^\dagger c_{6\alpha} c_{5\beta}^\dagger c_{4\beta} c_{3\gamma}^\dagger c_{2\gamma} + h.c.) - K_2 \sum_{\alpha\beta\gamma} (c_{1\alpha}^\dagger c_{2\alpha} c_{3\beta}^\dagger c_{4\beta} c_{5\gamma}^\dagger c_{6\gamma} + h.c.) + H_{\text{ex},\mathbf{R}}, \quad (5)$$

where the superexchange interaction is given as

$$H_{\text{ex},\mathbf{R}} = J \sum_{\langle\langle ij \rangle\rangle \in \circ_{\mathbf{R}}} (\mathbf{S}_i \cdot \mathbf{S}_j - \frac{1}{4}) n_i n_j. \quad (6)$$

It is interesting to note that the above superexchange differs from the usual form of the exchange interaction by having extra electron density operators n_i and n_j . This is because the positions of the electrons are not fixed due to their collective tunneling on the hexagon plaquette. The local Hilbert space of $H_{\circ_{\mathbf{R}}}$ also differs significantly from the on-site one for a conventional Mott insulator, and is instead spanned by the electron states that are labelled by both the positions and the spin quantum numbers of the three resonating electrons. Because the electrons are separated from each other by one lattice site due to the repulsive interaction, the Hilbert space for the electron positions is highly constrained. For the resonating hexagon centered at \mathbf{R} , there are in total 16 states that are labelled by

$$|\alpha\beta\gamma\rangle_A \equiv |n_1 = 0\rangle |n_2 = 1, \alpha\rangle |n_3 = 0\rangle \times |n_4 = 1, \beta\rangle |n_5 = 0\rangle |n_6 = 1, \gamma\rangle, \quad (7)$$

$$|\alpha\beta\gamma\rangle_B \equiv |n_1 = 1, \alpha\rangle |n_2 = 0\rangle |n_3 = 1, \beta\rangle \times |n_4 = 0\rangle |n_5 = 1, \gamma\rangle |n_6 = 0\rangle, \quad (8)$$

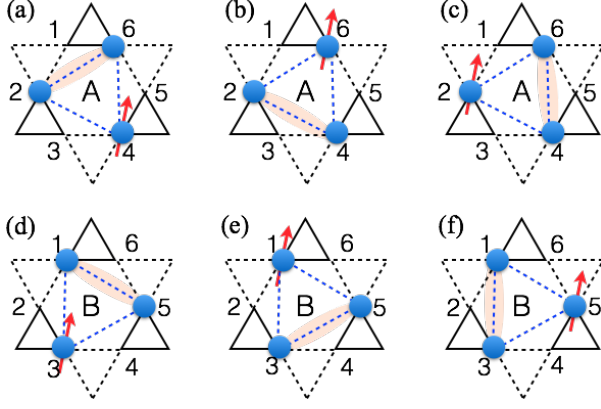


FIG. 3. (Color online.) Three spin-singlet positions for both A and B occupation configurations. The (orange) dimer refers to the spin singlet, and the (red) arrow is the dangling spin. The three spin-singlet configurations are related by the three-fold rotation around the hexagon center.

where α, β, γ ($=\uparrow, \downarrow$) refer to the electron spins at the occupied site. Since the hexagonal Hamiltonian $H_{\square\mathbf{R}}$ commutes with the total spin \mathbf{S}_{tot} and S_{tot}^z of the three resonating electrons, we use $\{S_{\text{tot}}, S_{\text{tot}}^z\}$ to label the spin states of the hexagon plaquette. From the spin composition rule for three electron spins, we have the following relation

$$\frac{1}{2} \otimes \frac{1}{2} \otimes \frac{1}{2} \equiv \frac{1}{2} \oplus \frac{1}{2} \oplus \frac{3}{2}, \quad (9)$$

where the left side are the product state of the three electron spins and the right side are the total spin states S_{tot} . For both A and B occupation configurations, there are eight spin states. Note that we have two pairs of $S_{\text{tot}} = 1/2$ states for each occupation configuration.

The two states with $S_{\text{tot}} = 3/2$ are simply the ferromagnetic states and are certainly not favored by the antiferromagnetic exchange interaction $H_{\text{ex},\mathbf{R}}$. Directly solving the Hamiltonian $H_{\square\mathbf{R}}$, we find that when

$$J > \frac{2}{3} [K_1 + K_2 - (K_1^2 - K_1 K_2 + K_2^2)^{\frac{1}{2}}], \quad (10)$$

the local ground states are four symmetric states with $S_{\text{tot}} = 1/2$. Here, the ‘‘symmetric’’ states refer to being symmetric between the A and B occupation configurations in Fig. 3. This is understood by the fact that the collective motion of three electrons favors symmetric states rather than antisymmetric ones. These four-fold degenerate states can be effectively characterized by two quantum numbers $\{s^z, \tau^z\}$ with $s^z = \pm\frac{1}{2}$ and $\tau^z = \pm\frac{1}{2}$, where s^z refers to the total spin $s^z \equiv S_{\text{tot}}^z = \pm\frac{1}{2}$. The pseudospin-1/2 operator $\boldsymbol{\tau}$ refers to the emergent orbitals that will be explained below.

The wavefunctions of the four degenerate states are labelled by $|\tau^z s^z\rangle_{\mathbf{R}}$ and are given as (to the order of

$\mathcal{O}(K_2/K_1)^{33}$),

$$|\uparrow\uparrow\rangle_{\mathbf{R}} = \frac{1}{2} [|\uparrow\uparrow\downarrow\rangle_{\text{A}} - |\uparrow\downarrow\uparrow\rangle_{\text{A}} + |\downarrow\uparrow\uparrow\rangle_{\text{B}} - |\uparrow\uparrow\downarrow\rangle_{\text{B}}], \quad (11)$$

$$|\downarrow\downarrow\rangle_{\mathbf{R}} = \frac{\sqrt{3}}{6} [2|\downarrow\uparrow\uparrow\rangle_{\text{A}} - |\uparrow\downarrow\uparrow\rangle_{\text{A}} - |\uparrow\uparrow\downarrow\rangle_{\text{A}} + 2|\uparrow\downarrow\uparrow\rangle_{\text{B}} - |\uparrow\uparrow\downarrow\rangle_{\text{B}} - |\downarrow\uparrow\uparrow\rangle_{\text{B}}], \quad (12)$$

and these other two states $|\uparrow\downarrow\rangle_{\mathbf{R}}$, $|\downarrow\uparrow\rangle_{\mathbf{R}}$ are simply obtained by applying a time-reversal transformation to the above two states,

$$|\uparrow\downarrow\rangle_{\mathbf{R}} = \frac{1}{2} [|\downarrow\downarrow\uparrow\rangle_{\text{A}} - |\downarrow\uparrow\downarrow\rangle_{\text{A}} + |\uparrow\downarrow\downarrow\rangle_{\text{B}} - |\downarrow\uparrow\uparrow\rangle_{\text{B}}], \quad (13)$$

$$|\downarrow\uparrow\rangle_{\mathbf{R}} = \frac{\sqrt{3}}{6} [2|\uparrow\uparrow\downarrow\rangle_{\text{A}} - |\downarrow\uparrow\downarrow\rangle_{\text{A}} - |\downarrow\downarrow\uparrow\rangle_{\text{A}} + 2|\downarrow\uparrow\downarrow\rangle_{\text{B}} - |\downarrow\downarrow\uparrow\rangle_{\text{B}} - |\uparrow\downarrow\downarrow\rangle_{\text{B}}]. \quad (14)$$

We clarify the physical origin of the four-fold degeneracy of the above four states for the hexagon plaquette. First, the two-fold degeneracy of $s^z = \pm 1/2$ is simply protected by the time-reversal symmetry. The remaining two-fold degeneracy comes from the point group symmetry of the resonating hexagon. This is ready to see if we fix the occupation configuration of the three electrons. To be more specific, let us start with the A configuration in the upper panel of Fig. 3. To optimize the antiferromagnetic exchange interaction, two electron spins out of the three must form a spin singlet, leaving the third electron as a dangling spin. As shown in Fig. 3, the spin singlet can be formed between any pair of the electrons, and the different arrangements of the spin singlet are related by the three-fold rotation. Although there seems to be three possible singlet arrangements, only two of them are linearly independent and are responsible for the two-fold degeneracy. Likewise, for the B configuration on the lower panel of Fig. 3, we again have two such degenerate states. When the three electrons start to move collectively within the hexagon between the A and B configurations, the corresponding states start to hybridize and the symmetric states are favored energetically. The two-fold degeneracy survives and is given as the $\tau^z = \uparrow, \downarrow$ states in Eqs. (11)-(14).

The three electrons are localized on the resonating hexagon but are delocalized within the resonating hexagon. It is hard for them to move out of the resonating hexagon, but easy for them to move within the resonating hexagon. Due to this collective motion, the wavefunctions of $|\tau^z s^z\rangle$ are extended and span across the resonating hexagon, and the $\tau^z = \uparrow, \downarrow$ states behave like two degenerate orbitals that are defined on the resonating hexagon. Since the degeneracy of $\tau^z = \uparrow, \downarrow$ states originate from the arrangements of the spin singlets, the pseudospin $\boldsymbol{\tau}$ is *even* under the time-reversal transformation. The two emergent orbital states that are defined in Eqs. (11) and (12) comprise the two-dimensional E-type

irreducible representation of the point group, and thus their two-fold degeneracy is protected by the point group symmetry of the resonating hexagon.

IV. THE KUGEL-KHOMSKII SPIN-ORBITAL INTERACTION

In this section we study and derive the interaction between the spins and the emergent orbitals that live on the neighboring resonating hexagons. This interaction is necessarily of the Kugel-Khomskii type. Based on the Kugel-Khomskii model, we obtain the Curie-Weiss temperature and Curie constant in the strong plaquette ordered regime, and compare with the high temperature results.

A. The Kugel-Khomskii model

The neighboring resonating hexagons are connected by a “bow-tie” structure that is composed of the corner-shared up and down triangles (see Fig. 4). The local moment interaction comes from the remaining exchange interaction between the two electron spins that reside on the four exterior vertices of the bow-tie. To illustrate the idea, we consider the bow-tie structure that connects the two resonating hexagons centered at \mathbf{R} and $\mathbf{R} + \mathbf{a}_1$ (see Fig. 1 and Fig. 4). To derive the local moment interaction, we need to project the remaining electron spin exchange interaction onto the four-fold degenerate local moment states $|\tau^z s^z\rangle$ of each resonating hexagon. For this purpose, we first write down the inter-hexagon exchange interaction between the electrons at the bow-tie vertices,

$$H'_{\text{ex}} = -\frac{J'}{4}[n_4(\mathbf{R}) + n_5(\mathbf{R})][n_1(\mathbf{R} + \mathbf{a}_1) + n_2(\mathbf{R} + \mathbf{a}_1)] \\ + J'[\mathbf{S}_4(\mathbf{R})n_4(\mathbf{R}) + \mathbf{S}_5(\mathbf{R})n_5(\mathbf{R})] \cdot [\mathbf{S}_1(\mathbf{R} + \mathbf{a}_1) \\ \times n_1(\mathbf{R} + \mathbf{a}_1) + \mathbf{S}_2(\mathbf{R} + \mathbf{a}_1)n_2(\mathbf{R} + \mathbf{a}_1)], \quad (15)$$

where we have included the exchange interactions for electrons at all four pairs of the external vertices. Again, since the position of the electron is not fixed, the electron number operator n_i is introduced. The exchange paths all go through the central vertex of the bow-tie and are of equal length. Therefore, only one exchange coupling J' is introduced for all the four pairs in Eq. (15). The exchange coupling J' can be obtained from the fourth order perturbation theory and is given as

$$J' = \frac{4t_1^2 t_2^2}{UV_1^2} + \frac{4t_1^2 t_2^2}{UV_2^2} + \frac{4t_1^2 t_2^2}{UV_1 V_2}, \quad (16)$$

and the fifth order perturbation theory could introduce more terms to J' without invoking double electron occupancy on a single lattice site. Moreover, since J' is the exchange coupling between the spins in the strong plaquette ordered regime, J' is expected to be weaker

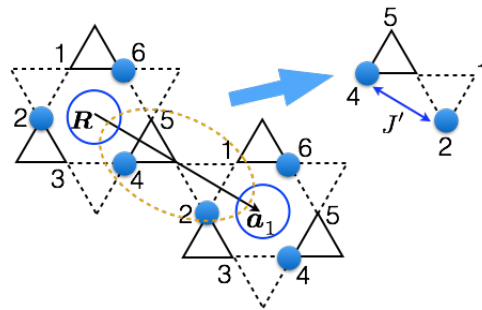


FIG. 4. (Color online.) The bow-tie structure that connects two neighboring resonating hexagons. In the upper right corner, we indicate the exchange interaction J' between two electrons.

than the intra-resonating-hexagon exchange coupling J in Eq. (6).

We project H'_{ex} onto the local ground state manifold at resonating hexagon sites \mathbf{R} and $\mathbf{R} + \mathbf{a}_1$ and then express the resulting interaction in terms of the spin \mathbf{s} and the pseudospin $\boldsymbol{\tau}$. The effective interaction on other bonds can be obtained likewise. The final local moment interaction reduces to a Kugel-Khomskii model³⁰ that is defined on the triangular lattice formed by the resonating hexagons. To the order of $\mathcal{O}(K_2/K_1)$, the Kugel-Khomskii model is given as

$$H_{\text{KK}} = \frac{J'}{9} \sum_{\mathbf{R}} \sum_{\mu=x,y,z} (\mathbf{s}_{\mathbf{R}} \cdot \mathbf{s}_{\mathbf{R}+\mathbf{a}_\mu}) \\ \times [1 + 4T_{\mathbf{R}}^\mu][1 - 2T_{\mathbf{R}+\mathbf{a}_\mu}^\mu], \quad (17)$$

where the new set of pseudospin operators, T^μ 's, are defined as

$$T_{\mathbf{R}}^x = -\frac{1}{2}\tau_{\mathbf{R}}^z - \frac{\sqrt{3}}{2}\tau_{\mathbf{R}}^x, \quad (18)$$

$$T_{\mathbf{R}}^y = -\frac{1}{2}\tau_{\mathbf{R}}^z + \frac{\sqrt{3}}{2}\tau_{\mathbf{R}}^x, \quad (19)$$

$$T_{\mathbf{R}}^z = \tau_{\mathbf{R}}^z, \quad (20)$$

and $\mathbf{a}_x = \mathbf{a}_1$, $\mathbf{a}_y = \mathbf{a}_2$ and $\mathbf{a}_z = -\mathbf{a}_1 - \mathbf{a}_2$. The particular expression of the Kugel-Khomskii model in Eq. (17) originates from the choice of two orbital wave functions in Eqs. (11)-(14). If a different set of orbital wave functions is chosen, the resulting Kugel-Khomskii model would have a different form. In Eq. (17), the effective exchange coupling is significantly reduced by after the projection compared to the original exchange coupling J' in Eq. (15). The important factor 1/9 in front of this equation can be understood physically as coming from the fact that each spin is found in the bowtie structure connecting two hexagons only 1/3 of the time.

B. The Curie-Weiss laws

Since the pseudospin $\boldsymbol{\tau}$ is even under the time reversal transformation and thus does not couple to the exter-

nal magnetic field, the low-temperature Curie-Weiss temperature thus detects the spin-spin interaction, and from the Kugel-Khomskii model H_{KK} we directly compute the Curie constant \mathcal{C} and the Curie-Weiss temperature Θ_{CW} at the low temperature,

$$\mathcal{C}^{\text{L}} = \frac{g^2 \mu_{\text{B}}^2 s(s+1) N}{3k_{\text{B}} 3}, \quad (21)$$

$$\Theta_{\text{CW}}^{\text{L}} = -\frac{2s(s+1)J'}{9}, \quad (22)$$

where N is the total number of electrons, g is the Landé factor, and “ $N/3$ ” in \mathcal{C}^{L} means the active spin degrees of freedom in the strong plaquette ordered phase comprise $1/3$ of the total number of electrons. This is a natural consequence due to the spin state reconstruction within each resonating hexagons. This result is consistent with the low-temperature magnetic susceptibility $\text{LiZn}_2\text{Mo}_3\text{O}_8$ ²¹⁻²⁴.

To make a comparison with the high-temperature susceptibility, we consider the high temperature regime where the plaquette charge order is present and the spin singlet within the resonating hexagon plaquette is thermally destroyed. In this regime, all the electron spins contribute to the magnetic susceptibility. Therefore, the Curie constant for this high-temperature regime is simply given by

$$\mathcal{C}^{\text{H}} = \frac{g^2 \mu_{\text{B}}^2 s(s+1) N}{3k_{\text{B}}}, \quad (23)$$

and is three times larger than the low-temperature one. Moreover, in this regime, Fig. 1 is a typical electron configuration. For each electron, there are four neighboring electrons that interact with this electron spin with the pairwise spin interaction across the bow-tie structure. Among these interactions, there are two intra-resonating-hexagon interactions with the coupling J and two inter-resonating-hexagon interaction J' . Then the Curie-Weiss temperature for this high-temperature regime is given as

$$\Theta_{\text{CW}}^{\text{H}} = -\frac{2s(s+1)}{3}(J+J'), \quad (24)$$

and is $3(1+J/J')$ times larger than the low-temperature one. Since J' is expected to be less than J , the ratio is larger than 6 and provides a separation of scale between the high temperature freezing of $2/3$ of the spins and the interaction among the remaining spins. In the experiment on $\text{LiZn}_2\text{Mo}_3\text{O}_8$, the two Curie-Weiss temperatures are -220K and -14K respectively²³.

V. PARTON CONSTRUCTION FOR THE CANDIDATE SPIN LIQUID STATE

Like any other spin-orbital exchange models³⁰, the Kugel-Khomskii model H_{KK} in our context involves the spin-spin interaction, the pseudospin-pseudospin interaction and the spin-pseudospin interaction, and all

these interactions are of the same energy scale. These interactions together make the model analytically intractable. In the absence of the spin-pseudospin interaction, the Heisenberg spin exchange model would favor the conventional 120-degree state with a long-range order. The spin-pseudospin interaction, however, competes with the Heisenberg term, destabilizes the conventional 120-degree state and may potentially induce a spin liquid state. This is because the quartic-like spin-pseudospin interaction allows the local moment to fluctuate more effectively in the spin-pseudospin space. Such a spin liquid, if exists, may be smoothly connected to the $U(1)$ spin liquid with spinon Fermi surfaces that was proposed for the weak plaquette charge ordered regime in Ref. 6.

From the experimental side, a broad continuous excitation has been discovered in the inelastic neutron scattering measurement on powder samples. The authors in Ref. 21 proposed a gapless spin liquid state. Moreover, the neutron spectral weight in the experiment is not suppressed at low energies, which indicates that the ground state cannot be a Dirac spin liquid. Based on the experimental results, we here propose the candidate ground state to a spin liquid with a spinon Fermi surface. This phenomenological proposal is again consistent with the previous suggestion from the weak coupling approach⁶. To demonstrate the phenomenological consequence of this proposal, we develop a new parton construction that is designed for our spin-orbital model and suggest the experimental consequence of this candidate state.

A. The parton construction

There are both spin and orbital degrees of freedom on a single site \mathbf{R} . To account for both of them, we introduce the following fermionic parton representation,

$$\tau_{\mathbf{R}} = \sum_{m,n} \sum_{\alpha} \frac{1}{2} f_{\mathbf{R}m\alpha}^{\dagger} \sigma_{mn} f_{\mathbf{R}n\alpha}, \quad (25)$$

$$\mathbf{s}_{\mathbf{R}} = \sum_m \sum_{\alpha,\beta} \frac{1}{2} f_{\mathbf{R}m\alpha}^{\dagger} \sigma_{\alpha\beta} f_{\mathbf{R}m\beta}, \quad (26)$$

where $m, n = \uparrow, \downarrow$ refer to the pseudospin state for the orbitals, $\alpha, \beta = \uparrow, \downarrow$ refer to the spin state, and $\sigma = (\sigma^x, \sigma^y, \sigma^z)$ is the vector of Pauli matrices. To get back to the physical Hilbert space, we further impose a Hilbert space constraint

$$\sum_{\alpha} \sum_m f_{\mathbf{R}m\alpha}^{\dagger} f_{\mathbf{R}m\alpha} = 1. \quad (27)$$

Unlike the pure spin model, our spinon carries an extra orbital index. This parton construction could be well extended to other spin-orbital models.

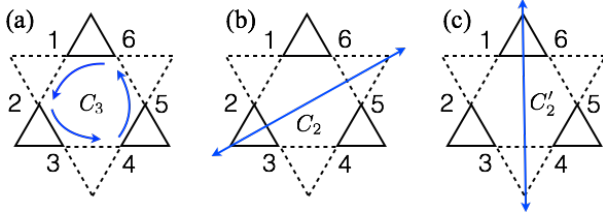


FIG. 5. (a) Three fold rotation around the center of the plaquette. (b) The two fold rotation axis. (c) Another two fold rotation axis.

B. The symmetry property of the spinons

The U(1) spin liquid with spinon Fermi surfaces was proposed for the weak plaquette charge ordered regime⁶. For this state, the spinon transforms identically like the electron under the lattice transformation, and there is no projective realization of the lattice symmetry. Since we suggest that the possible spin liquid for our Kugel-Khomskii model in the strong coupling regime is connected to the ground state in the weak plaquette ordered regime, we here explicitly derive the symmetry transformation of the spinons in our context.

Let us consider a single plaquette at \mathbf{R} , the symmetries include the three-fold rotation C_3 and two two-fold rotations C_2 and C'_2 (see Fig. 5). The lattice symmetry does not change the spin component, but acts on the orbital degree of freedom. Under C_3 , the lattice sites within the hexagon plaquette transform as

$$C_3 : 2 \rightarrow 4, 4 \rightarrow 6, 6 \rightarrow 2, \quad (28)$$

$$C_3 : 1 \rightarrow 3, 3 \rightarrow 5, 5 \rightarrow 1, \quad (29)$$

therefore, from the orbital wavefunctions, we have that the states $|\uparrow\uparrow\rangle_{\mathbf{R}}$ and $|\downarrow\downarrow\rangle_{\mathbf{R}}$ transform as

$$C_3 : |\uparrow\uparrow\rangle_{\mathbf{R}} \rightarrow -\frac{1}{2}|\uparrow\uparrow\rangle_{\mathbf{R}} + \frac{\sqrt{3}}{2}|\downarrow\downarrow\rangle_{\mathbf{R}}, \quad (30)$$

$$C_3 : |\downarrow\downarrow\rangle_{\mathbf{R}} \rightarrow -\frac{\sqrt{3}}{2}|\uparrow\uparrow\rangle_{\mathbf{R}} - \frac{1}{2}|\downarrow\downarrow\rangle_{\mathbf{R}}, \quad (31)$$

where the transformation does not depend on the spin quantum number, and the identical transformations are obtained for the states $|\uparrow\downarrow\rangle_{\mathbf{R}}$ and $|\downarrow\uparrow\rangle_{\mathbf{R}}$. One then establishes

$$C_3 : f_{\mathbf{R}\uparrow\alpha} \rightarrow -\frac{1}{2}f_{\mathbf{R}\uparrow\alpha} + \frac{\sqrt{3}}{2}f_{\mathbf{R}\downarrow\alpha}, \quad (32)$$

$$C_3 : f_{\mathbf{R}\downarrow\alpha} \rightarrow -\frac{\sqrt{3}}{2}f_{\mathbf{R}\uparrow\alpha} - \frac{1}{2}f_{\mathbf{R}\downarrow\alpha}. \quad (33)$$

Following the same type of calculation, under C_2 and C'_2 , we have

$$C_2 : 5 \leftrightarrow 6, 1 \leftrightarrow 4, 2 \leftrightarrow 3, \quad (34)$$

and

$$C_2 : f_{\mathbf{R}\uparrow\alpha} \rightarrow -f_{\mathbf{R}\uparrow\alpha}, \quad (35)$$

$$C_2 : f_{\mathbf{R}\downarrow\alpha} \rightarrow +f_{\mathbf{R}\downarrow\alpha}, \quad (36)$$

and

$$C'_2 : 1 \leftrightarrow 6, 2 \leftrightarrow 5, 3 \leftrightarrow 4, \quad (37)$$

and

$$C'_2 : f_{\mathbf{R}\uparrow\alpha} \rightarrow +\frac{1}{2}f_{\mathbf{R}\uparrow\alpha} - \frac{\sqrt{3}}{2}f_{\mathbf{R}\downarrow\alpha}, \quad (38)$$

$$C'_2 : f_{\mathbf{R}\downarrow\alpha} \rightarrow -\frac{\sqrt{3}}{2}f_{\mathbf{R}\uparrow\alpha} - \frac{1}{2}f_{\mathbf{R}\downarrow\alpha}. \quad (39)$$

C. The spinon Fermi surface state

From the spinon symmetry properties, we determine the generic symmetry allowed spinon mean-field Hamiltonian H_{spinon} ,

$$H_{\text{spinon}} = \sum_{\mathbf{R}, \mu} \sum_{m, n} \sum_{\alpha} t_{mn}^{\mu} f_{\mathbf{R}m\alpha}^{\dagger} f_{\mathbf{R}+\mathbf{a}_{\mu}, n, \alpha} + h.c., \quad (40)$$

where t_{mn}^{μ} is a bond dependent hopping matrix for the spinons, and we have the symmetry allowed hoppings as

$$t^x = -\tilde{t}_1 \mathbb{1}_{2 \times 2} + \tilde{t}_2 \sigma^z + \sqrt{3} \tilde{t}_2 \sigma^x, \quad (41)$$

$$t^y = -\tilde{t}_1 \mathbb{1}_{2 \times 2} + \tilde{t}_2 \sigma^z - \sqrt{3} \tilde{t}_2 \sigma^x, \quad (42)$$

$$t^z = -\tilde{t}_1 \mathbb{1}_{2 \times 2} - 2\tilde{t}_2 \sigma^z, \quad (43)$$

and $\mathbb{1}_{2 \times 2}$ is a 2×2 identity matrix. This model describes the spinon hopping on the triangular lattice with two orbitals at each lattice site. Since the spinons are at 1/4 filling, each band is partially filled and the system develops spinon Fermi surfaces (see Fig. 6). The mean-field ground state is obtained by filling the spinon states below the Fermi energy E_F ,

$$|\Psi_{\text{MF}}\rangle = \prod_{E_{\mathbf{k}, j} < E_F} \xi_{\mathbf{k}j\uparrow}^{\dagger} \xi_{\mathbf{k}j\downarrow}^{\dagger} |0\rangle, \quad (44)$$

where $E_{\mathbf{k}, j}$ is the energy of the eigenmode that is defined by $\xi_{\mathbf{k}j\uparrow}^{\dagger}$ or $\xi_{\mathbf{k}j\downarrow}^{\dagger}$, and is given as

$$E_{\mathbf{k}, 1} = -2\tilde{t}_1(c_x + c_y + c_z) + 4|\tilde{t}_2|(c_x^2 + c_y^2 + c_z^2 - c_y c_z - c_x c_z - c_x c_y)^{\frac{1}{2}}, \quad (45)$$

$$E_{\mathbf{k}, 2} = -2\tilde{t}_1(c_x + c_y + c_z) - 4|\tilde{t}_2|(c_x^2 + c_y^2 + c_z^2 - c_y c_z - c_x c_z - c_x c_y)^{\frac{1}{2}}. \quad (46)$$

Here $c_{\mu} = \cos(\mathbf{k} \cdot \mathbf{a}_{\mu})$.

D. The qualitative feature of the spinon continuum due to the emergent orbitals

The key property for the spinon mean-field model is the presence of the inter-orbital hopping \tilde{t}_2 that hybridizes different orbitals such that each spinon band no longer has a definite orbital character. This inter-orbital spinon hopping arises from the fact that the orbital interaction is anisotropic in the orbital space and only respects the

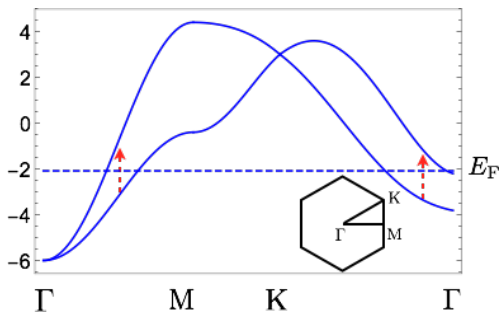


FIG. 6. (Color online.) The two spinon bands and their vertical particle-hole transition between the two bands. In the plot, $\tilde{t}_2 = 0.3\tilde{t}_1$, and $\tilde{t}_1 = 1$ is used as the energy unit. The inset is the Brillouin zone of the triangular lattice formed by the resonating hexagons.

discrete lattice symmetry. In the inelastic neutron scattering, the neutron would only see the effective spin and not see the emergent orbital degree of freedom. The orbital degree of freedom, however, has an important effect on the spinon continuum that is observed by inelastic neutron scattering. The neutron detects the particle-hole excitation across the spinon Fermi level. From the momentum and energy conservation, we have the momentum and energy transfer of the neutron as

$$\mathbf{q} = \mathbf{q}_1 - \mathbf{q}_2, \quad (47)$$

$$E = E_{\mathbf{q}_1, j_1} - E_{\mathbf{q}_2, j_2}, \quad (48)$$

where \mathbf{q}_1 and $E_{\mathbf{q}_1, j_1}$ are the momentum and the energy of an unoccupied spinon while \mathbf{q}_2 and $E_{\mathbf{q}_2, j_2}$ are the momentum and the energy of the filled spinon. The particle-hole excitation would involve both the intra-band transitions (with $j_1 = j_2$) and the inter-band transitions (with $j_1 \neq j_2$). If there is no orbital degree of freedom and there is only one single spinon band, the inter-band transition is not involved, and the inelastic neutron scattering spectral weight for the intra-band transition is suppressed for the finite energies at the Γ point. This is because at the mean-field level the intra-band process always excites the finite-energy spinon particle-hole pair with a finite momentum. In contrast, with the inter-band vertical process (see Fig. 6), the spinon particle-hole pair with zero momentum can carry a wide range of finite energies. In Fig. 7, we explicitly compute the energy and momentum spread of the contribution to spin-spin correlation function as measured by neutron scattering due to the spinon particle-hole pair excitation for the specific choice of spinon hoppings. Qualitatively a broad continuum is observed, with a small amount of missing weight near the Γ point due to features of the inter-band transition.

VI. EMERGENT ORBITAL ORDER IN A FIELD

Despite the possible exotic spin liquid ground state at zero field, the Kugel-Khomskii model H_{KK} becomes more

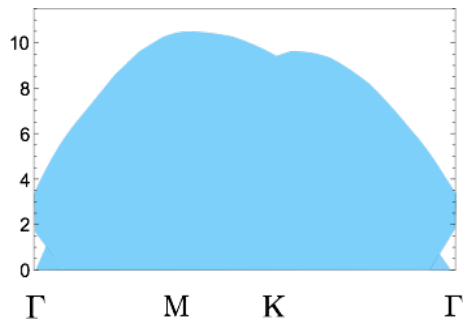


FIG. 7. (Color online.) The spinon continuum contribution to the spin spin correlation function as measured by neutron scattering along high symmetry momentum direction. Due to the inter-band transition, there exists the spinon continuum up to finite energies near the Γ point, with a small region of missing weight. The energy parameters here are the same as the ones in Fig. 6.

tractable in the presence of a strong external magnetic field. Due to the suppression of the exchange coupling in H_{KK} , it is feasible to choose the magnetic fields to fully polarize the local spin moments such that $s^z = \uparrow$ for every resonating hexagon, but at the same time keep the field from polarizing all the electron spins in the kagome system. The pseudospin τ is not directly effected by the magnetic field since it does not couple to the Zeeman field. The pseudospins remain active, and the interaction between them turns out to be a ferromagnetic compass model on the triangular lattice formed by the resonating hexagons,

$$H_{\text{RKK}} = -\frac{2J'}{9} \sum_{\mathbf{R}} \sum_{\mu=x,y,z} T_{\mathbf{R}}^{\mu} T_{\mathbf{R}+\mathbf{a}_{\mu}}^{\mu}. \quad (49)$$

From a standard Luttinger-Tisza type of mean-field approach³⁴, we find that the mean-field ground state of H_{RKK} has an accidental U(1) continuous degeneracy, *i.e.* any ferro-orbital ($\mathbf{q} = \mathbf{0}$) state with the pseudospin τ orienting in xz plane is a classical ground state. Here, we parametrize the mean-field pseudospin order as

$$\tau_{\text{cl}} = \frac{1}{2}(\cos \theta \hat{z} + \sin \theta \hat{x}) \quad (50)$$

with $\theta \in [0, 2\pi)$.

This continuous U(1) ground state degeneracy at the mean-field level of the reduced Kugel-Khomskii model H_{RKK} is lifted when the quantum fluctuations of the orbitals are included. We study this quantum order by disorder phenomenon from the linear orbital-wave theory. Here we introduce the Holstein-Primakoff boson to represent the pseudospin operator $\tau_{\mathbf{R}}$ as follows,

$$\tau_{\mathbf{R}} \cdot \hat{\tau}_{\text{cl}} = \frac{1}{2} - a_{\mathbf{R}}^{\dagger} a_{\mathbf{R}}, \quad (51)$$

$$\tau_{\mathbf{R}} \cdot \hat{y} = \frac{1}{2i} [a_{\mathbf{R}} - a_{\mathbf{R}}^{\dagger}], \quad (52)$$

$$\tau_{\mathbf{R}} \cdot (\hat{y} \times \hat{\tau}_{\text{cl}}) = \frac{1}{2} [a_{\mathbf{R}} + a_{\mathbf{R}}^{\dagger}], \quad (53)$$

where $\hat{\tau}_{\text{cl}} \equiv \boldsymbol{\tau}_{\text{cl}}/|\boldsymbol{\tau}_{\text{cl}}|$ is the orientation of the pseudospin. We keep the quadratic terms in the Holstein-Primakoff boson operators and express the reduced Kugel-Khomskii model as

$$H_{\text{RKK}} = \sum_{\mathbf{k} \in \text{BZ}} [2A_{\mathbf{k}} a_{\mathbf{k}}^\dagger a_{\mathbf{k}} + B_{\mathbf{k}} (a_{\mathbf{k}} a_{-\mathbf{k}} + h.c.)] + E_{\text{cl}}, \quad (54)$$

where ‘‘BZ’’ refers to the Brioullin zone of the triangular lattice formed by the resonating hexagon plaquettes and

$$E_{\text{cl}} = -\frac{J' N}{12 \cdot 3}, \quad (55)$$

$$A_{\mathbf{k}} = \frac{2J'}{9} \left[-\frac{\sin^2(\theta - \pi/3)}{4} \cos(\mathbf{k} \cdot \mathbf{a}_x) - \frac{\sin^2(\theta + \pi/3)}{4} \cos(\mathbf{k} \cdot \mathbf{a}_y) - \frac{\sin^2 \theta}{4} \cos(\mathbf{k} \cdot \mathbf{a}_z) + \frac{3}{4} \right], \quad (56)$$

$$B_{\mathbf{k}} = \frac{2J'}{9} \left[-\frac{\sin^2(\theta - \pi/3)}{4} \cos(\mathbf{k} \cdot \mathbf{a}_x) - \frac{\sin^2(\theta + \pi/3)}{4} \cos(\mathbf{k} \cdot \mathbf{a}_y) - \frac{\sin^2 \theta}{4} \cos(\mathbf{k} \cdot \mathbf{a}_z) \right], \quad (57)$$

The linear orbital-wave Hamiltonian is then diagonalized by a Bogoliubov transformation for the Holstein-Primakoff bosons and is given by

$$H_{\text{RKK}} = E_{\text{cl}} + \sum_{\mathbf{k} \in \text{BZ}} \left[\frac{\omega_{\mathbf{k}}}{2} - A_{\mathbf{k}} \right] + \sum_{\mathbf{k} \in \text{BZ}} \omega_{\mathbf{k}} \alpha_{\mathbf{k}}^\dagger \alpha_{\mathbf{k}},$$

where the orbital-wave (or ‘orbitor’) mode reads

$$\omega_{\mathbf{k}} = 2(A_{\mathbf{k}}^2 - B_{\mathbf{k}}^2)^{\frac{1}{2}}. \quad (58)$$

From Eq. (58), the quantum correction to the ground state energy is

$$\Delta E = \sum_{\mathbf{k} \in \text{BZ}} \left[\frac{\omega_{\mathbf{k}}}{2} - A_{\mathbf{k}} \right]. \quad (59)$$

In Fig. 8, we plot the quantum correction as a function of the angular parameter θ . The minima occur at

$$\theta = \frac{\pi}{6} + \frac{n\pi}{3}, \quad n \in \mathcal{Z}, \quad (60)$$

and are indicated in Fig. 9a.

Since the two-fold orbital degeneracy arises from the point group symmetry, the emergent orbital order, that breaks the orbital degeneracy, has to be related to the symmetry breaking. To understand the physical consequence of the orbital order, we consider the following product state wavefunction that is appropriate for the $\mathbf{q} = \mathbf{0}$ ferro-orbital state,

$$|\Psi\rangle_{\text{orb}} = \prod_{\mathbf{R}} \left[\cos \frac{\theta}{2} |\uparrow\uparrow\rangle_{\mathbf{R}} + \sin \frac{\theta}{2} |\downarrow\downarrow\rangle_{\mathbf{R}} \right], \quad (61)$$

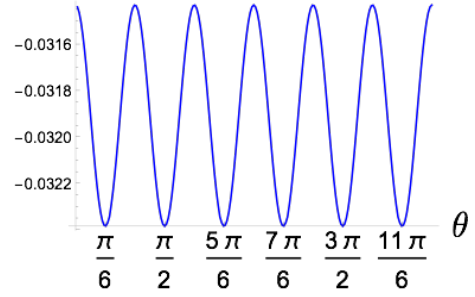


FIG. 8. The quantum zero-point energy per resonating hexagon for the mean-field orbital order. The energy unit is set to $2J'/9$ in the figure.

This variational wavefunction gives the orbital ordering in Eq. (50). From this wavefunction, we find that the electron density is uniform at every site within each resonating hexagon and thus preserves the rotation and reflection symmetries. We then compute the local magnetization for each site within the resonating hexagon,

$$\langle s_1^z \rangle_{\mathbf{R}} = \langle s_6^z \rangle_{\mathbf{R}} = \frac{1}{12} + \frac{\sin(\theta - \pi/6)}{6}, \quad (62)$$

$$\langle s_2^z \rangle_{\mathbf{R}} = \langle s_3^z \rangle_{\mathbf{R}} = \frac{1}{12} + \frac{\sin \theta}{6}, \quad (63)$$

$$\langle s_4^z \rangle_{\mathbf{R}} = \langle s_5^z \rangle_{\mathbf{R}} = \frac{1}{12} - \frac{\sin(\theta + \pi/6)}{6}. \quad (64)$$

Although the total local magnetization of each resonating hexagon is $\langle s^z \rangle_{\mathbf{R}} = \sum_{i=1}^6 \langle s_i^z \rangle_{\mathbf{R}} = 1/2$, the orbital ordering leads to a modulation of the spin ordering inside

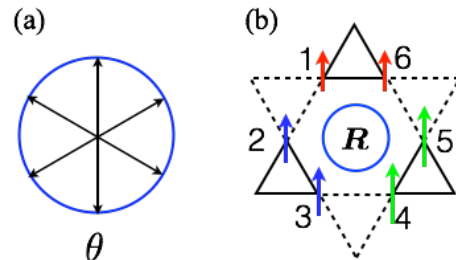


FIG. 9. (Color online.) (a) The selection of the θ on a unit circle by quantum fluctuation. The arrow indicates the optimal choice. (b) The magnetic moment distribution within the resonating hexagon for $\theta = \pi/6$. It is clear that the three-fold rotation about the center of the hexagon is broken.

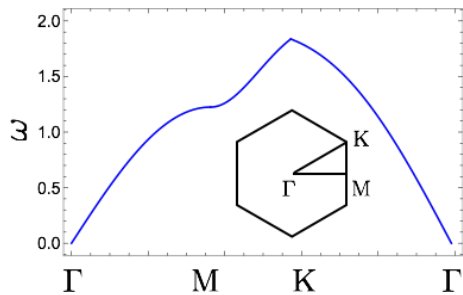


FIG. 10. The orbiton dispersion along the high-symmetry momentum line. The inset is the Brillouin zone of the triangular lattice formed by the resonating hexagons. The energy unit is set to $2J'/9$ in the figure.

each resonating hexagon (see Fig. 9b). The three-fold rotational symmetry about the center of the resonating hexagon is explicitly broken by the orbital ordering.

In Fig. 10, we plot the dispersion of the orbiton excitation for $\theta = \pi/6$. We find the dispersion is gapless at the Γ point due to the breaking of the accidental $U(1)$ degeneracy. This pseudo-Goldstone mode is expected to be gapped if the interaction between the Holstein-Primakoff bosons is included. Since the interaction induced gap should be very small compared to the orbiton energy scale, one would expect to observe the heat capacity $C_v \sim T^2$ at low temperatures.

VII. DISCUSSION

We discuss the experimental consequences of the plaquette charge order, the emergent orbitals, and the orbital orders. The plaquette charge order explicitly breaks the lattice translation symmetry and would lead to some variation of the bond lengths according to the symmetry breaking. This may be detected by high-resolution X-ray scattering or X-ray pair distribution function (PDF) measurement. The plaquette charge order reconstructs the spin states within each resonant hexagon leading to the freezing of $2/3$ of the spins, as observed in the spin susceptibility in $\text{LiZn}_2\text{Mo}_3\text{O}_8$ ^{21–25}. A different explanation of the susceptibility anomaly in $\text{LiZn}_2\text{Mo}_3\text{O}_8$ based on the lattice distortion and the emergent lattices has been proposed in a previous work²⁶. Both this previous work and the current work require a translation symmetry breaking by tripling the crystal unit cell. Such a translation symmetry breaking has not yet been observed in the experiment. Here we point out the possible reason, namely, that under certain conditions, the symmetry breaking must be short range at all temperatures.

The Li ion is mobile and may make the system slightly off stoichiometry. To accommodate the missing or extra charges, the system needs to create domain walls within the symmetry broken phase. An example of such domain walls is shown in Fig. 11 for the case when the filling is slightly more than $1/6$. Each solid dot represents the

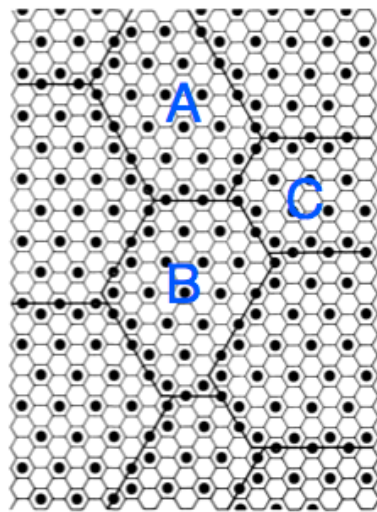


FIG. 11. A picture of the domain walls separating the ABC domains when the electron occupation is off-stoichiometry, in this case slightly more than $1/6$ per Mo.

charge order shown in Fig. 1. Note that the charge order can be centered on one of three hexagons, thereby forming ABC type domains. A certain density of domain walls will be required for a given deviation from $1/6$ filling. There is an energy cost per unit length of the domain wall, because electrons are now forced to occupy neighboring sites. The resulting state is expected to be a “liquid” state with an exponential decay of correlations for the electron charge density²⁷. This result is special for the hexagonal arrangement of domain walls and the reason is as follows. It was pointed out by J. Villain³⁵, there exists a breathing mode that expands or shrinks one particular domain but costs no energy because the total domain wall length is not changed. This is illustrated in Fig. 12. Consequently the free energy of the system of domain walls is purely entropic and is proportional to temperature T . In the long wavelength limit, the elastic constant of the system is also proportional to T and so is the energy to create a dislocation. An example of a dislocation is shown in Fig. 13. By the usual Berezinski-Kosterlitz-Thouless (BKT) argument, the competition of this energy with the entropy associated with the dislocation determines whether the dislocation will proliferate, resulting in an exponentially decaying correlation function. Unlike the usual BKT argument, where the dislocation energy is a constant and a phase transition is predicted at a finite temperature, here the result depends on the numerical coefficient of the linear T term in the elastic energy. A detailed computation carried out in Ref. 27 showed that the system is always disordered at any temperature. A short range charge ordering makes the detection more difficult, but not impossible. Perhaps resonant X-ray scattering which couples directly to the electrons will have a better chance seeing this distortion.

The emergent orbital is a degree of freedom that naturally emerges from the plaquette charge order on the

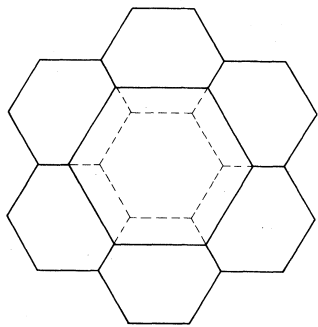


FIG. 12. The breathing mode of Villain. Note that the total wall length and hence its energy has not changed. This mode contribute only to the entropy.

breathing Kagome lattice. The presence of this extra degree of freedom distinguishes the current proposal from the previous one in Ref. 26. However, the emergent orbital is not detectable in the magnetization measurement since the orbital does not couple directly to the external magnetic field. However, it does contribute to the heat capacity and the entropy. We expect an additional entropy from the emergent orbitals apart from the spin entropy. This extra entropy from the orbitals may be measurable on the high-quality samples. The suggested spinon Fermi surface ground state and the spinon excitation should be detectable via inelastic neutron scattering. In fact, the existing measurement does suggest a broad continuum of excitations²¹, even though the measurement was taken on powder samples. Since the qualitative feature for the spinon inter-band particle-hole excitation is more visible at the Γ point, optical measurement or Raman scattering can be useful for detecting the finite energy spinon continuum at the Γ point.

A magnetic field that is of the order of the low-temperature Curie-Weiss temperature is expected to polarize the spin degree of freedom. The magnetic field should be much less than the high temperature Curie-Weiss temperature to prevent polarizing the spins that form the spin singlet within the resonating hexagon. The remaining orbital degrees of freedom then develop an orbital order via a quantum order by disorder mechanism and support a pseudo-Goldstone mode that gives a heat capacity $C_v \sim T^2$ at low temperatures. The orbital wave excitation may be detected by the resonant inelastic X-ray scattering. The orbital order creates a magnetic moment redistribution within the resonating hexagon. This intra-hexagon static magnetic structure may be detected by high-resolution neutron scattering, μ SR and/or NMR measurements.

Finally, there exists a large family of cluster magnets in which the electrons are localized on the cluster units and form CMI^{5-13,19,20}. The physical properties of many of these cluster magnets have not been explored carefully.

Recently, 1T-TaS₂ is proposed as a QSL candidate¹². In this system, the low-temperature (commensurate) charge

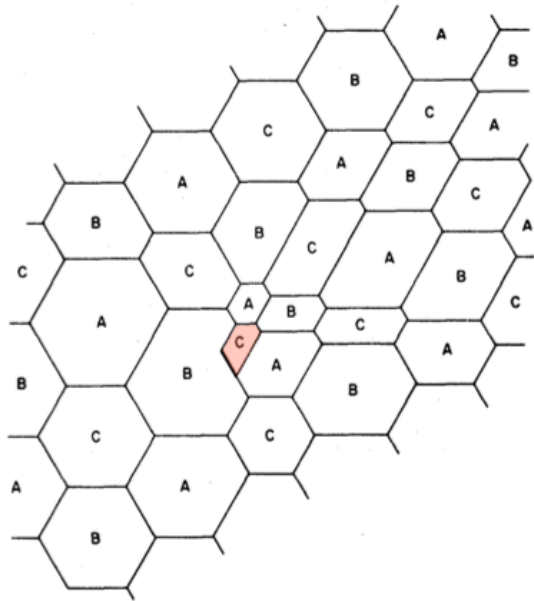


FIG. 13. A picture of a dislocation center (in red) in the system of domain walls.

density wave order enlarges the unit cell such that there exists one localized and unpaired electron inside the 13-site David-star cluster. This system can thus be considered as a CMI¹². These clusterly localized electrons form effective spin-1/2 local moments that interact with each other and may develop a spin liquid ground state¹². Besides these two-dimensional cluster magnets, the Ta-based and Mo-based lacunar spinels are good examples of three dimensional CMIs^{5,9-11}. In these materials, the systems naturally host a breathing pyrochlore lattice structure where one half of the tetrahedral clusters is smaller than the other half and host the localized electrons⁵. The study on these systems are quite limited so far. We expect that the cluster localization of the electrons in these CMIs may bring some interesting phenomena and enriches our understanding of Mott physics.

VIII. ACKNOWLEDGMENTS

G.C. is supported by the ministry of science and technology of China with the grant No.2016YFA0301001, the reserach initiative funds and the program of first-class university construction of Fudan University, and the thousand-youth-talent program of China. P.A.L. is supported by the U. S. National Science Foundation under DMR-1522575.

- ¹ William Witczak-Krempa, Gang Chen, Yong Baek Kim, and Leon Balents, “Correlated Quantum Phenomena in the Strong Spin-Orbit Regime,” *Annual Review of Condensed Matter Physics* **5**, 57–82 (2014).
- ² S. Maekawa, T. Tohyama, S.E. Barnes, S. Ishihara, W. Koshibae, and G. Khaliullin, *Physics of Transition Metal Oxides*, Springer Series in Solid-State Sciences (Springer-Verlag Berlin Heidelberg, Berlin Heidelberg, 2004).
- ³ Y. Tokura and N. Nagaosa, “Orbital physics in transition-metal oxides,” *Science* **288**, 462–8 (2000).
- ⁴ Giniyat Khaliullin, “Orbital order and fluctuations in mott insulators,” *Prog. Theor. Phys. Supplement* **160**, 155–202 (2005).
- ⁵ Gang Chen, Hae-Young Kee, and Yong Baek Kim, “Fractionalized charge excitations in a spin liquid on partially filled pyrochlore lattices,” *Phys. Rev. Lett.* **113**, 197202 (2014).
- ⁶ Gang Chen, Hae-Young Kee, and Yong Baek Kim, “Cluster mott insulators and two curie-weiss regimes on an anisotropic kagome lattice,” *Phys. Rev. B* **93**, 245134 (2016).
- ⁷ Jian-Ping Lv, Gang Chen, Youjin Deng, and Zi Yang Meng, “Coulomb liquid phases of bosonic cluster mott insulators on a pyrochlore lattice,” *Phys. Rev. Lett.* **115**, 037202 (2015).
- ⁸ Juan Carrasquilla, Gang Chen, and Roger G. Melko, “Tripartite entangled plaquette state in a cluster magnet,” *Phys. Rev. B* **96**, 054405 (2017).
- ⁹ M. M. Abd-Elmeguid, B. Ni, D. I. Khomskii, R. Pocha, D. Johrendt, X. Wang, and K. Syassen, “Transition from Mott Insulator to Superconductor in GaNb_4Se_8 and GaTa_4Se_8 under High Pressure,” *Phys. Rev. Lett.* **93**, 126403 (2004).
- ¹⁰ Daigorou Hirai, Martin Bremholm, Jared M. Allred, Jason Krizan, Leslie M. Schoop, Qing Huang, Jing Tao, and R. J. Cava, “Spontaneous Formation of Zigzag Chains at the Metal-Insulator Transition in the β -Pyrochlore CsW_2O_6 ,” *Phys. Rev. Lett.* **110**, 166402 (2013).
- ¹¹ Heung-Sik Kim, Jino Im, Myung Joon Han, and Hosub Jin, “Spin-orbital entangled molecular j_{eff} states in lacunar spinel compounds,” *Nature Communications* **5**, 3988 (2014).
- ¹² K.T. Law and Patrick A. Lee, “1T-TaS₂ as a quantum spin liquid,” *PNAS* **114**, 6996–7000 (2017).
- ¹³ Paolo G. Radaelli, Y. Horibe, Matthias Gutmann, Hiroki Ishibashi, C. H. Chen, Richard M. Ibberson, Y. Koyama, Yew-San Hor, Valery Kiryukhin, and Sang-Wook Cheong, “Formation of isomorphous Ir^{3+} and Ir^{4+} octamers and spin dimerization in the spinel CuIr_2S_4 ,” *Nature* **416**, 155–158 (2002).
- ¹⁴ F. Pollmann, P. Fulde, and K. Shtengel, *Phys. Rev. Lett.* **100**, 136404 (2008).
- ¹⁵ S. V. Isakov, S. Wessel, R. G. Melko, K. Sengupta, and Yong Baek Kim, “Hard-core bosons on the kagome lattice: Valence-bond solids and their quantum melting,” *Phys. Rev. Lett.* **97**, 147202 (2006).
- ¹⁶ Frank Pollmann, Krishanu Roychowdhury, Chisa Hotta, and Karlo Penc, “Interplay of charge and spin fluctuations of strongly interacting electrons on the kagome lattice,” *Phys. Rev. B* **90**, 035118 (2014).
- ¹⁷ Karim Ferhat and Arnaud Ralko, “Phase diagram of the $\frac{1}{3}$ -filled extended hubbard model on the kagome lattice,” *Phys. Rev. B* **89**, 155141 (2014).
- ¹⁸ Andreas Rüegg and Gregory A. Fiete, “Fractionally charged topological point defects on the kagome lattice,” *Phys. Rev. B* **83**, 165118 (2011).
- ¹⁹ Philippe Gall, Rabih Al Rahal Al Orabi, Thierry Guizouarn, and Patrick Gougeon, “Synthesis, crystal structure and magnetic properties of $\text{Li}_2\text{InMo}_3\text{O}_8$: A novel reduced molybdenum oxide containing magnetic Mo_3 clusters,” *Journal of Solid State Chemistry* **208**, 99 – 102 (2013).
- ²⁰ C. C. Torardi and R. E. McCarley, “Synthesis, crystal structures, and properties of lithium zinc molybdenum oxide ($\text{LiZn}_2\text{Mo}_3\text{O}_8$), zinc molybdenum oxide ($\text{Zn}_3\text{Mo}_3\text{O}_8$), and scandium zinc molybdenum oxide ($\text{ScZnMo}_3\text{O}_8$), reduced derivatives containing the Mo_3O_{13} cluster unit,” *Inorganic Chemistry* **24**, 476–481 (1985).
- ²¹ M. Mourigal, W. T. Fuhrman, J. P. Sheckelton, A. Wartelle, J. A. Rodriguez-Rivera, D. L. Abernathy, T. M. McQueen, and C. L. Broholm, *Phys. Rev. Lett.* **112**, 027202 (2014).
- ²² J. P. Sheckelton, F. R. Foronda, LiDong Pan, C. Moir, R. D. McDonald, T. Lancaster, P. J. Baker, N. P. Armitage, T. Imai, S. J. Blundell, and T. M. McQueen, *Phys. Rev. B* **89**, 064407 (2014).
- ²³ J. P. Sheckelton, J. R. Neilson, D. G. Soltan, and T. M. McQueen, *Nature Materials* **11**, 493–496 (2012).
- ²⁴ J.P. Sheckelton, J.R. Neilson, and T.M. McQueen, “Electronic tunability of the frustrated triangular-lattice cluster magnet $\text{LiZn}_{2-x}\text{Mo}_3\text{O}_8$,” *Mater. Horiz.* **2**, 76–80 (2015).
- ²⁵ A. Akbari-Sharabaf, R. Sinclair, A. Verrier, D. Ziat, H. D. Zhou, X. F. Sun, and J. A. Quilliam, “Tunable quantum spin liquidity in the $1/6$ th-filled breathing kagome lattice,” arXiv:1709.01904 (2017).
- ²⁶ Rebecca Flint and Patrick A. Lee, *Phys. Rev. Lett.* **111**, 217201 (2013).
- ²⁷ S. N. Coppermith, Daniel S. Fisher, B. I. Halperin, P. A. Lee, and W. F. Brinkman, “Dislocations and the commensurate-incommensurate transition in two dimensions,” *Phys. Rev. B* **25**, 349–363 (1982).
- ²⁸ Olexei I. Motrunich, *Phys. Rev. B* **72**, 045105 (2005).
- ²⁹ Sung-Sik Lee and Patrick A. Lee, *Phys. Rev. Lett.* **95**, 036403 (2005).
- ³⁰ K. I. Kugel and D. I. Khomskii, *Sov. Phys. Usp.* **25**, 231 (1982).
- ³¹ R. Moessner, S. L. Sondhi, and P. Chandra, “Phase diagram of the hexagonal lattice quantum dimer model,” *Phys. Rev. B* **64**, 144416 (2001).
- ³² F. Pollmann, P. Fulde, and K. Shtengel, “Kinetic ferromagnetism on a kagome lattice,” *Phys. Rev. Lett.* **100**, 136404 (2008).
- ³³ We expect that $V_1 \gtrsim V_2, t_1 > t_2$, so $K_1 \gg K_2$ for $\text{LiZn}_2\text{Mo}_3\text{O}_8$.
- ³⁴ J. M. Luttinger and L. Tisza, “Theory of dipole interaction in crystals,” *Phys. Rev.* **70**, 954–964 (1946).
- ³⁵ J. Villain, in “Ordering in Strongly Fluctuating Condensed Matter Systems”, edited by T. Riste (Plenum, New York, 1980), p. 221.